University of Glasgow

Colonia, S., Leble, V., Steijl, R., and Barakos, G. (2017) Assessment and calibration of the γ equation transition model for a wide range of Reynolds numbers at low Mach. *AIAA Journal*, (doi:10.2514/1.J055403)

This is the author's final accepted version.

There may be differences between this version and the published version. You are advised to consult the publisher's version if you wish to cite from it.

http://eprints.gla.ac.uk/130763/

Deposited on: 31 October 2016

Enlighten – Research publications by members of the University of Glasgow
http://eprints.gla.ac.uk

Assessment and Calibration of the $\gamma-$Equation Transition Model for a Wide Range of Reynolds Numbers at Low Mach

S. Colonia, V. Leble, R. Steijl and G. Barakos

School of Engineering, University of Glasgow, Glasgow G12 8QQ, Scotland

Abstract

The numerical simulation of flows over large-scale wind turbine blades without considering the transition from laminar to fully turbulent flow may result in incorrect estimates of the blade loads and performance. Thanks to its relative simplicity and promising results, the Local-Correlation based Transition Modelling concept represents a valid way to include transitional effects into practical CFD simulations. However, the model involves coefficients to be tuned to match the required application. In this paper, the $\gamma-$equation transition model is assessed and calibrated, for a wide range of Reynolds numbers at low Mach, as needed for wind turbine applications. Different aerofoils are used to evaluate the original model and calibrate it; while a large scale wind turbine blade is employed to show that the calibrated model can lead to reliable solution for complex three-dimensional flows. The calibrated model shows promising results for both two-dimensional and three-dimensional flows, even if cross-flow instabilities are neglected.

Introduction

In many engineering applications, flow computations without considering the transition from laminar to fully turbulent flow may result in incorrect predictions. Thus, the significance of the transition process in various aerodynamics applications can not be understated, and proper prediction of boundary layer transition is vital in aerodynamic design. Nevertheless, methods for simulating transitional flows are still not used frequently in computational fluid dynamics.

The main types of transition are natural and bypass. Natural transition process occurs at low free-stream turbulence intensity (Tu), usually less than 1%. In the initial stage, known as receptivity, environmental disturbances, such as free-stream noise and turbulence and surface roughness, propagate as small perturbations within the boundary layer. For 2D flows, these instabilities take the form of periodic waves, known as Tollmien-Schlichting (TS) waves, which, when the momentum-thickness Reynolds number (Re_θ) exceeds a critical threshold, are gradually amplified in the laminar boundary layer. Their evolution is well captured by the linear stability theory; however, as these instabilities grow, they begin to exhibit non-linear interactions leading rapidly to the breakdown to turbulence. In 3D boundary layers, the mean velocity

profile also displays a cross-flow (CF) component other than the stream-wise. The stream-wise velocity profile generates waves similar to the TS waves observed in 2D flow, while the cross-flow velocity profile induces CF waves that propagate in a direction normal to the free-stream. Although the same linear stability theory is applicable to both wave types, the non-linear interactions are different for TS and CF instabilities [1] . In various situations, laminar to turbulent transition occurs at Reynolds numbers lower than what predicted by the linear stability theory, this suggests that another transition mechanism exists. Indeed, if the laminar boundary layer is exposed to large free-stream turbulence levels, larger than 1%, bypass transition process occurs. The term bypass means that the natural transition mechanism driven by the TS or CF waves has been short-circuited and the disturbances are amplified by non-linear phenomena.

Direct Numerical Simulation (DNS) and sometimes Large Eddy Simulation (LES) [2] are probably the most suitable approaches for transition prediction, however the computational cost of these methods is too high for routine engineering applications and are used mainly for research purpose.

At present, the most popular methods for predicting transition are the ones based on the linear stability theory such as the e^N model developed more than half a century ago by Smith and Gamberoni [3] and by van Ingen [4] . This approach uses the linear stability theory to calculate the growth of the disturbance amplitude in the boundary layer. The so-called N factor represents the total growth rate of the most unstable among the disturbances and it is not universal. The e^N method has been successfully used to predict transition for a wide range of test cases. However, the main obstacle to its use with the current Computational Fluid Dynamics (CFD) methods lies in the complex infrastructure required to apply the model. Indeed, the stability analysis is applied on velocity profiles predicted from highly resolved boundary-layer codes and the steps required can be summarised as follows: the output of a boundary-layer method is employed as input for the stability analysis which then provides the required information to the turbulence model in the Reynolds Averaged Navier-Stokes (RANS) CFD solver. This makes the approach difficult to employ in complex 3D flows; thus the development of simplified methods is of unquestionable practical interest.

An alternative to this approach is to use the concept of intermittency, γ, which represents the fraction of time that the flow is turbulent during the transition phase. The intermittency is zero in the laminar region and becomes one in the fully turbulent region, thus can be used to control the onset and the development of transition. From experimental observations, the development of intermittency is almost general for the steady boundary layer on a flat plate, therefore the onset location can be correlated. Most correlations usually relate the transition momentum thickness Reynolds number to turbulence intensity and the pressure gradient. Among them, the most commonly used are the correlation of Abu-Ghannam and Shaw [5] , Michel's criterion [6] and the Cebeci and Smith approach [7] . Dhawan and Narasimha [8] were the first to correlate experimental data and propose a general intermittency distribution function across flow transition. Their correlation was later improved by Gostelow et al. [9] including flows with pressure gradients for a range of free-stream turbulence intensities. Steelant and Dick [10] proposed to obtain the intermittency more generally as the solution of a transport equation in which the source term is defined so that the γ distribution of Dhawan and Narasimha [8] is reproduced across the transition region. In [10] , the intermittency was then incorporated into two strongly coupled sets of conditioned Navier-Stokes equations and this is not compatible with the currently available CFD codes. In [11] , Suzen and Huang formulated an alternative

transport equation for the intermittency based on Steelant and Dick [10] , and the work of Cho and Chung [12] . These approaches, although empirical, are often sufficiently accurate for capturing the major effects of transition. Moreover, they are relatively easy to calibrate and correlations can be developed for the different transition mechanisms such as bypass, natural, cross-flow and separation induced transition. However, these models typically require information on the integral thickness of the boundary layer and the state of the flow outside the boundary layer and these non-local operations are not well adapted to massively parallel computations.

For these reasons, the Local-Correlation based Transition Modelling (LCTM) concept was proposed by Menter et. al. [13] almost a decade ago and fully disclosed by the authors later in [14] . The first formulation of the LCTM, termed γ-Re$_\theta$ model, involves two additional transport equations, for the turbulence intermittency and for the transition onset correlation respectively, which allow combining experimental correlations in a local fashion with the underlying turbulence model. A strong characteristic of the LCTM concept is its flexibility and relatively straightforward implementation into practical CFD simulations allowing the inclusion of different transitional effects for which enough experimental data is available to tune and optimise the model. Since its introduction, the correlation based transition model has shown promising results and various works have been done to improve it. Recently, a simplified version of the model has been presented [15] with the goal to maintain the LCTM concept, including the ability to model various transitional processes, reduce the formulation to only the γ-equation providing tunable coefficients to match the required application, and obtain a Galilean invariant formulation. In [15] , Menter et al. assessed the model for different test cases covering a range of Reynolds number between 50×10^3 and 500×10^3 at subsonic and transonic Mach numbers. Thus, further works are needed to evaluate the γ-equation model at more extreme conditions such as high Reynolds numbers (i.e. $Re \geq 1 \times 10^6$), very low Reynolds numbers (i.e. $Re \leq 50 \times 10^3$) and supersonic/hypersonic flows.

In this paper, the $\gamma-$equation transition model is calibrated for all Reynolds numbers flows at low Mach numbers to be employed for wind turbine applications, allowing for better estimates of flow transition. For wind turbine applications, flow analysis and design methods based on the RANS equations have been extensively employed by several research groups [16] . The most common approach is to use fully turbulent simulations ignoring the transition process. However, fully turbulent flow solutions have been shown to over-predict the aerodynamic drag impacting the design of wind turbine aerofoils [17–19] . Brodeur and van Dam [17] demonstrated the validity of the e^N method for two-dimensional flows around wind turbine profiles. As mentioned before, the complex infrastructure required by the methods affect it applicability to complex three-dimensional cases. For this reason, Sørensen [18] , first, and Khayatzadeh and Nadarajah [19] , later, made an effort to use the γ-Re$_\theta$ model to predict laminar-turbulent transition for wind turbine aerofoils and rotors showing promising results.

In the context of the present work, the $\gamma-$equation transition model of Menter has been implemented in the CFD code of the University of Glasgow, HMB3 [20,21] . A detailed description of the solver is presented in section 2. In section 3 the main features as well as the tunable constants of the model are discussed. Then, section 4 contains a summary of the selected test cases while in section 5 the calibration approach and the results are presented. During the calibration of the model, various test cases have been simulated. The goal was not to obtain perfect agreement with experimental data and

linear stability results, since this would require to change the model correlation with more complex ones, but to tolerate some differences as part of the approach taken to formulate the original model [15] . Finally, in section 6 conclusions of the present work are given as well as suggestions for future improvements.

Fully Implicit Formulation for a Steady Case

The Helicopter Multi-Block (HMB3) code [21] , developed at Glasgow University, has been used in the present work. The RANS equations are discretised using a cell-centred finite volume approach. The computational domain is divided into a finite number of control-volumes, and the governing equations are applied in integral-conservation form at each cell. The equations are written in a curvilinear co-ordinate system. The spatial discretisation of the system equations leads to a set of ordinary differential equations in time. The solver uses a fully-implicit time integration where the new solution does not only depend on the known solution at the previous time step, but also on a coupling between the cell variables at the new time step. Thus, following the pseudo-time approach, after the linearisation of the residual at the new pseudo time step the discretised RANS result in a large system of linear equations which, rewritten in terms of the primitive variables **P**, for a steady is given by

$$\left[\frac{V_{i,j,k}}{\Delta t^*}\frac{\partial \mathbf{W}_{i,j,k}}{\partial \mathbf{P}_{i,j,k}} + \frac{\partial \mathbf{R}_{i,j,k}}{\partial \mathbf{P}_{i,j,k}}\right]\Delta \mathbf{P}_{i,j,k} = -\mathbf{R}_{i,j,k}(\mathbf{W}^m) \tag{1}$$

where **R** represents the residual vector. The above equation must be solved over the computational domain and provides an update to the vector of primitive variables variables as a solution of a system of algebraic equations of the form $Ax-b=0$. In HMB3, the latter is solved employing a Generalised Conjugate Gradient (GCG) method [22] with an Incomplete Lower Upper factorisation (ILU) pre-conditioner [23] .

For the evaluation of the inviscid fluxes, the code implements the Roe's [24] and Osher's schemes [25] for subsonic and transonic flows but also the LM-Roe [26] and AUSM$^+$/AUSM^+up [27] schemes are available for very low and high Mach flows [28,29] . The Osher's scheme is used in the present work. For the viscous fluxes the solver employs a second order central discretisation scheme.

To discretise the convective part of the Navier-Stokes equations a, formally, third order Monotone Upstream-Centred Scheme for Conservation Laws (MUSCL) [30] is employed with the Van Albada limiter [31] . To avoid ill-conditioning a first order Jacobian is used. Thus, the exact Jacobian matrix is approximated by removing the dependence of the MUSCL interpolation This leads to a lower quality Jacobian which, however, is much more computationally efficient. Indeed, it has been experienced that the conditioning of the system gets worse when additional off-diagonal terms are included.

When a transition model is in use the resulting Jacobian matrix is given by

$$\begin{bmatrix} A_{00} & A_{01} & A_{02} \\ A_{10} & A_{11} & A_{12} \\ A_{20} & A_{21} & A_{22} \end{bmatrix} \tag{2}$$

where

- A_{00} is a 5×5 matrix associated with the flow primitive variables,
- A_{11} is a 2×2 matrix for a two-equation turbulence model,
- A_{11} is a scalar or a 2×2 matrix for one-equation or two-equation transition models,
- A_{01} and A_{10} are related to how the fluid variables depend on the turbulent variables and vice-versa,
- A_{02} and A_{20} are related to how the fluid variables depend on the transition model variables and vice-versa,
- A_{12} and A_{21} are related to how the turbulent variables depend on the transition model variables and vice-versa.

The $\gamma-$Equation Transition Model

For the complete definition of the $\gamma-$equation LCTM the reader is referred to the original work of Menter et al. [15] whose notation is preserved in the present paper. A first set of parameters is the one used in the critical momentum-thickness Reynolds number correlation

$$Re_{\theta_c}\left(Tu_L, \lambda_{\theta L}\right) = C_{TU1} + C_{TU2} \exp\left(-C_{TU1} Tu_L F_{PG}\left(\lambda_{\theta L}\right)\right) \tag{3}$$

and define the minimum (C_{TU1}), maximum ($C_{TU1} + C_{TU2}$) and the rate of decay with an increase of the turbulence intensity (C_{TU3}) of the critical Re_{θ_c} number. A further set of constants is introduced in the function employed to include in the transition onset the effect of the stream-wise pressure gradient

$$F_{PG}\left(\lambda_{\theta L}\right) = \begin{cases} min\left(1 + C_{PG1}\lambda_{\theta L}, C_{PG2}^{lim}\right) & \lambda_{\theta L} \geq 0 \\ \\ min\left(1 + C_{PG2}\lambda_{\theta L}, C_{PG2}^{lim}\right) & \lambda_{\theta L} < 0 \end{cases} \tag{4}$$

Here, C_{PG1} controls the value of Re_{θ_c} in areas with favorable pressure while C_{PG2} with adverse pressure gradient. In [15] also an additional constant C_{PG3} is considered to correct Re_{θ_c} in regions with separation if necessary but it is set to zero and here the same approach is followed.

The authors believe that a further tunable parameter, here named C_{onset1}, can be identified in the function that controls the transition onset as follow

$$F_{onset1} = \frac{Re_v}{C_{onset1} Re_{\theta_c}} \quad \text{with} \quad C_{onset1} = 2.2. \tag{5}$$

Since the triggering of the transition is based on Re_v instead of Re_θ computed from the velocity profile, C_{onset1} should change accordingly with the ratio between these two Reynolds numbers. This ratio can be expressed as function of the shape factor, H, or the pressure gradient parameter λ_θ. In the original model the value 2.2 is selected to achieve a F_{onset1} equal to one within a Blasius boundary layer and this effect is taken into account through the correlation for the critical

momentum-thickness Reynolds number presented in equation (3). However, previous works [14,19] for the γ-Re$_\theta$ model observed the necessity to re-scale C_{onset1} at high Reynolds numbers.

For the results shown in the present work, the model has been coupled with the $k-\omega$ SST turbulence model of Menter [32] and the Kato-Launder formulation [33] of the production term is employed. To eliminate the non-physical decay of turbulence variables in the freestream for external aerodynamic problems, the additional sustaining terms to the equations of the SST model have been employed [34] .

Test Cases Description

For the calibration of the model and its assessment, with particular focus on wind turbine applications, two different aerofoils and a wind turbine blade have been used. All aerofoil computations are performed at Mach numbers typical of wind turbine applications, i.e. Ma 0.1. Three different operative conditions, summarised in table 1, are considered for the wind turbine blade.

The first aerofoil selected is the DU00-w-212, an aerofoil currently employed in the AVATAR project for large scale wind turbines [35] . The computational domain can be seen in figure 1. The domain is divided in 70 blocks and 82 thousands cells with 331 cells around the aerofoil, 155 cells in the normal direction and 103 cells from the TE to the far-field. The employed normal spacing in terms of the chord, c, at the wall is $1 \times 10^{-6}c$, while spacings of $1 \times 10^{-3}c$ and $1 \times 10^{-4}c$ are used around the aerofoil at the leading (LE) and trailing (TE) edges, respectively.

The second profile used for the present work is the NASA/Langley/Somers NLF(1)-0416 natural laminar flow aerofoil. This aerofoil is designed for general aviation applications and typically operates at Reynolds numbers beteween 1×10^6 and 9×10^6. The computational grid is shown in figures 2 and consists in a multi-block structured grid of 75 thousands cells divided in 32 blocks. Around the aerofoil and in the normal direction 275 and 171 cells are used, respectively, while 85 cells are employed from the TE to the far-field. In this case the same spacings as for the DU00-w-212 aerofoil are employed.

In all aerofoil computations the far-field is placed at a distance $40c$, where c is the aerofoil chord.

Finally, the AVATAR wind turbine blade [35] is selected as 3D case. Figures 3 and 4 show a sketch of the blade and a section cut. The grid consists of 15 millions cells with 325 points around the section, 295 in the span-wise direction and 101 in the normal direction. The number of blocks in which the domain is decomposed is 442 and the spacing at the wall is $5 \times 10^{-7}c_{max}$. In this case the far-field is placed at 6 blade radius towards the outflow and 3 blade radius towards the inflow and in the radial direction.

In all considered geometries, hyperbolic laws are employed for the cells distributions along all the blocks' edges and steady-state simulations have been performed.

Wind speed, U_W (m/s)	RMP	Pitch
10.00	8.6	0.00
10.50	9.0	0.00
12.00	9.6	3.98

Table 1 – Summary of the selected operative conditions for the AVATAR wind turbine blade (RPM: rotations per minute).

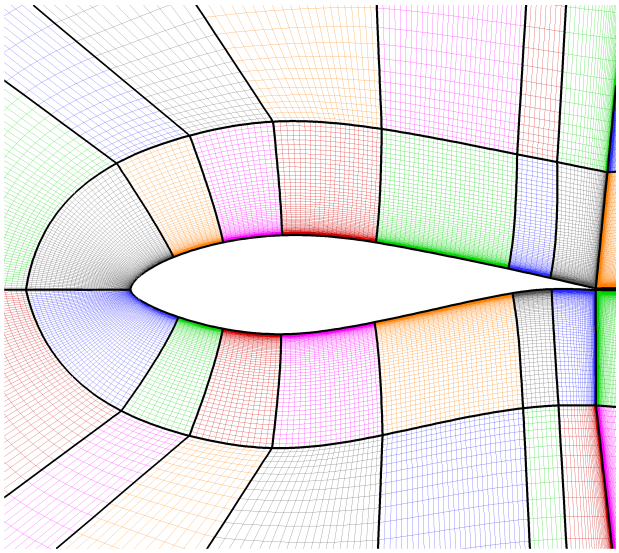

Figure 1 – DU00-w-212 aerofoil

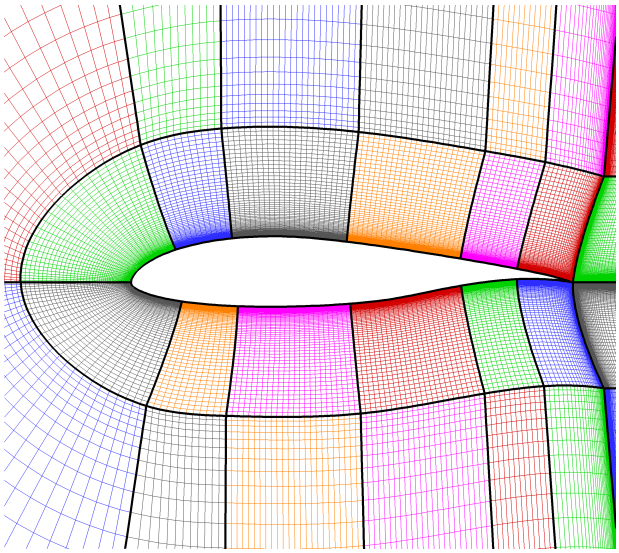

Figure 2 – NLF(1)-0416 aerofoil.

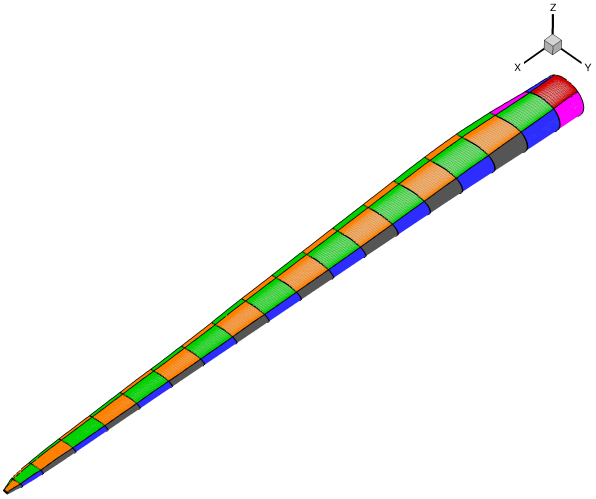

Figure 3 – AVATAR wind turbine blade

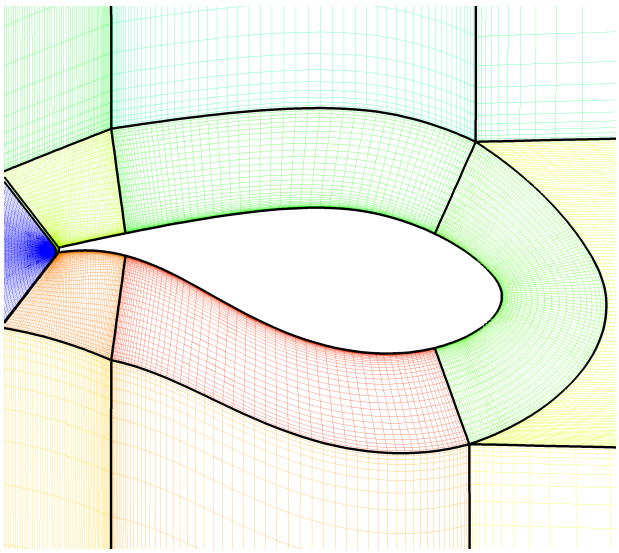

Figure 4 – AVATAR blade section at 75% radius.

Assessment and Calibration of the $\gamma-$equation Model

2-D Cases

In the present work, only natural transition, i.e. $Tu < 1\%$, is considered at high Reynolds numbers and cross-flow instabilities are neglected. The first proposed modification to the model constants is a rescaling of C_{TU1} and C_{TU2} in equation (4) from 100.0 and 1000.0 to 163.0 and 1002.25, respectively. The choice of this constants is done so that equation (3) exactly matches the Abu-Ghannam and Shaw correlation [5] for zero pressure gradient, i.e. $\lambda_{\theta L} = 0$. Furthermore, the minimum value of 163.0 for the critical momentum-thickness Reynolds number, Re_{θ_c}, is in accordance with the Tollmien-Schlichting limit of stability [5] .

For the flow around the DU00-w-212 aerofoil at high Reynolds numbers, no experimental data is currently available in the literature so simulations performed with Xfoil [36] are employed here as benchmark. Xfoil is a well known tool for 2D aerofoil computations, firstly developed at the Massachusetts Institute of Technology in the 1980s and since then widely used by companies and research institutes. The reason behind the choice of this tool is that it employs the e^N method to predict the transition position.

Figures 5a-c show the skin friction coefficient on the lower and upper surfaces of the aerofoil, as functions of the position along the chord, for different high Reynolds numbers at low free-stream turbulence intensity $Tu = 0.0816\%$. The results of the original model are in reasonable agreement with Xfoil predictions only at $Re = 3\times10^6$ as shown in figure 5a. When the Reynolds further increases, the original model predicts too early transition as can be observed in figures 5b-g. The first proposed modification improved the agreement of the model with Xfoil predictions at $Re = 3 \times 10^6$; however, it was not enough at higher Reynolds numbers.

As mentioned in section 3, previous works in the literature for the γ-Re$_\theta$ model have observed that the constant employed in the ratio defined in equation 5 needs to be increased [14,19] . Thus, a gradual increase of the constant C_{Onset1} to 2.75, 3.3, 3.85 and 4.4 has been considered here. In figures 6a-c skin friction predictions are provided for different values of C_{Onset1}. The results show that an optimal range of C_{Onset1}, which leads to a good agreement with Xfoil's e^N results, can be found at each Reynolds number.

In figure 7 the optimal values of C_{Onset1}, among the ones employed, are reported for the considered Reynolds numbers, while a summary of all the modified constants can be found in table 2. Looking at figure 7, it is possible to notice that a simple logarithmic curve fitting can be given as follows

$$C_{onset1} = min(4.84, max(2.2, 1.388ln(Re \times 10^{-6}) + 0.705)) \tag{6}$$

to define C_{Onset1} as a function of the Reynolds number for $1 \times 10^6 \leq Re \geq 15 \times 10^6$. In the original model [15] , Menter et al. observed that the ratio

$$\frac{Re_v}{2.2Re_\theta} \tag{7}$$

can change by as much as a factor of around 2.2 for typical values of the boundary layer shape factor. For this reason a maximum value of 4.84 is employed here for C_{Onset1}, while the minimum value of 2.2 is used to recover the transition onset of the original model for $Re < 3 \times 10^6$. Figures 8a-c show predictions of the skin friction coefficient on the lower and upper surfaces of the DU00-w-212 aerofoil for different Reynolds numbers with equation (6) employed. The results are in very good agreement with the predictions obtained using the e^N method for all the Reynolds numbers considered.

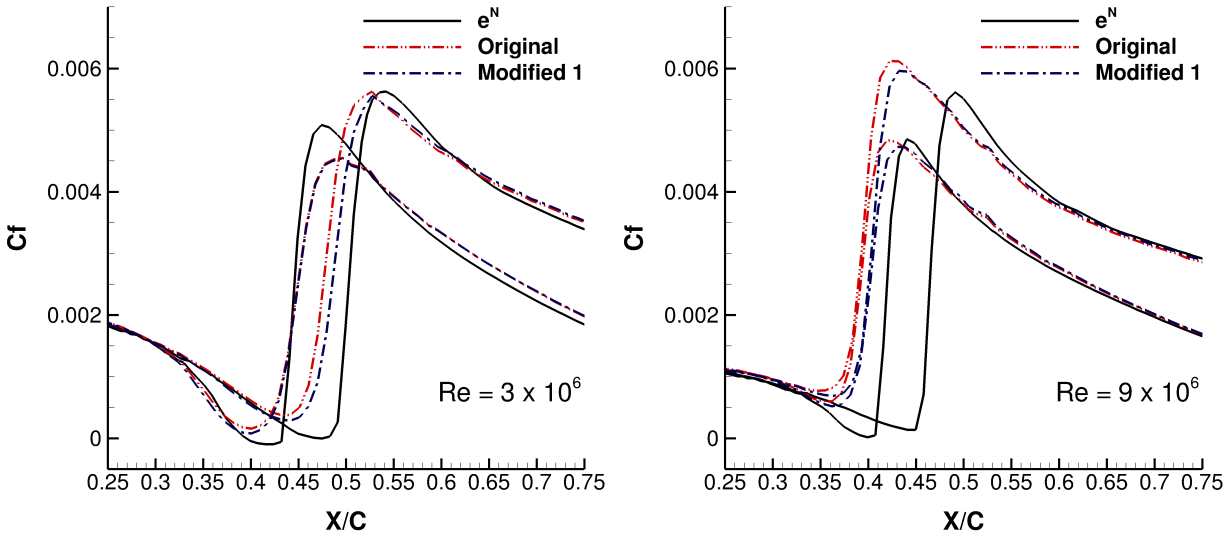

(a) $Re = 3 \times 10^6$.

(b) $Re = 9 \times 10^6$.

(c) $Re = 15 \times 10^6$.

Figure 5 – Skin friction coefficient, C_f, at various Reynolds numbers: effect of the proposed $C_{TU1} = 163.0$ and $C_{TU2} = 1002.25$ on the predicted transition region. DU00-w-212 aerofoil at $Ma = 0.1$ and free-stream $Tu = 0.0816\%$ and $\mu_t/\mu = 1.0$.

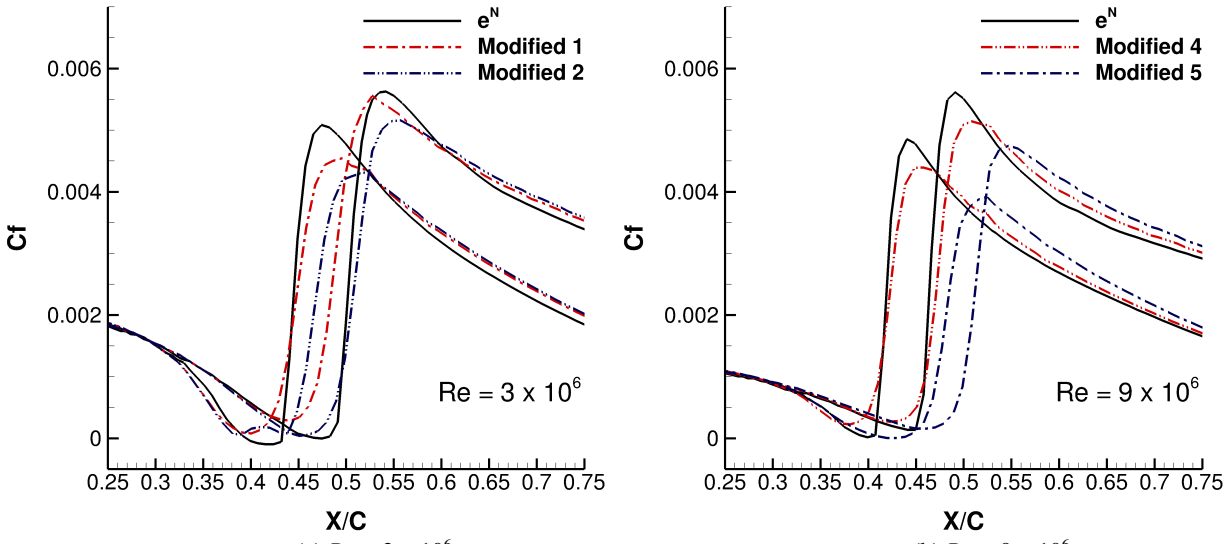

(a) $Re = 3 \times 10^6$.

(b) $Re = 9 \times 10^6$.

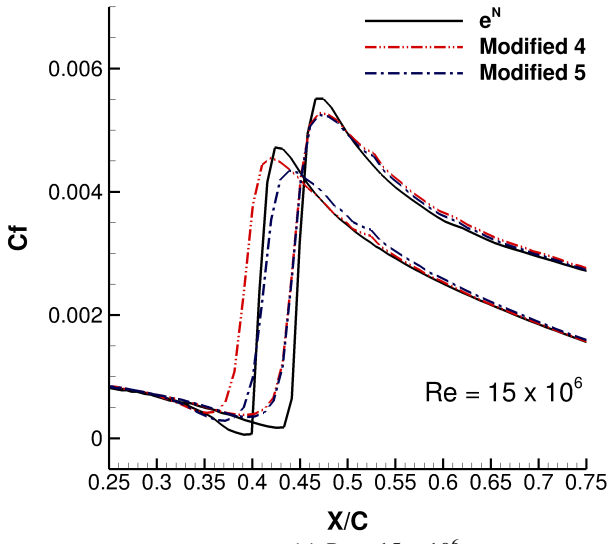

(c) $Re = 15 \times 10^6$.

Figure 6 – Skin friction coefficient, C_f, at various Reynolds numbers: effect of C_{Onset1} on the predicted transition region. DU00-w-212 aerofoil at $Ma = 0.1$ and free-stream $Tu = 0.0816\%$ and $\mu_t/\mu = 1.0$.

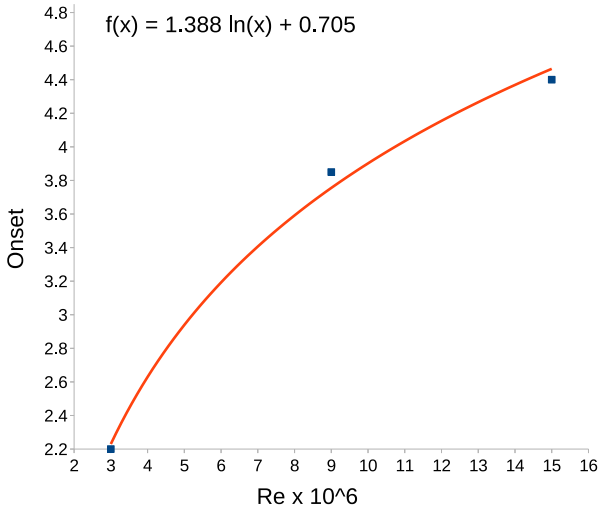

Figure 7 – Proposed logarithm curve fitting for C_{onset1} at $3 \times 10^6 \leq Re \geq 15 \times 10^6$.

Model	C_{TU1}	C_{TU2}	C_{onset1}
Original	100.00	1000.00	2.20
Modified 1	163.00	1002.25	2.20
Modified 2	163.00	1002.25	2.75
Modified 3	163.00	1002.25	3.30
Modified 4	163.00	1002.25	3.85
Modified 5	163.00	1002.25	4.40
Log. Fit.	163.00	1002.25	$min(4.84, max(2.2, 1.388ln(Re \times 10^{-6}) + 0.705))$

Table 2 – Summary of the employed constants.

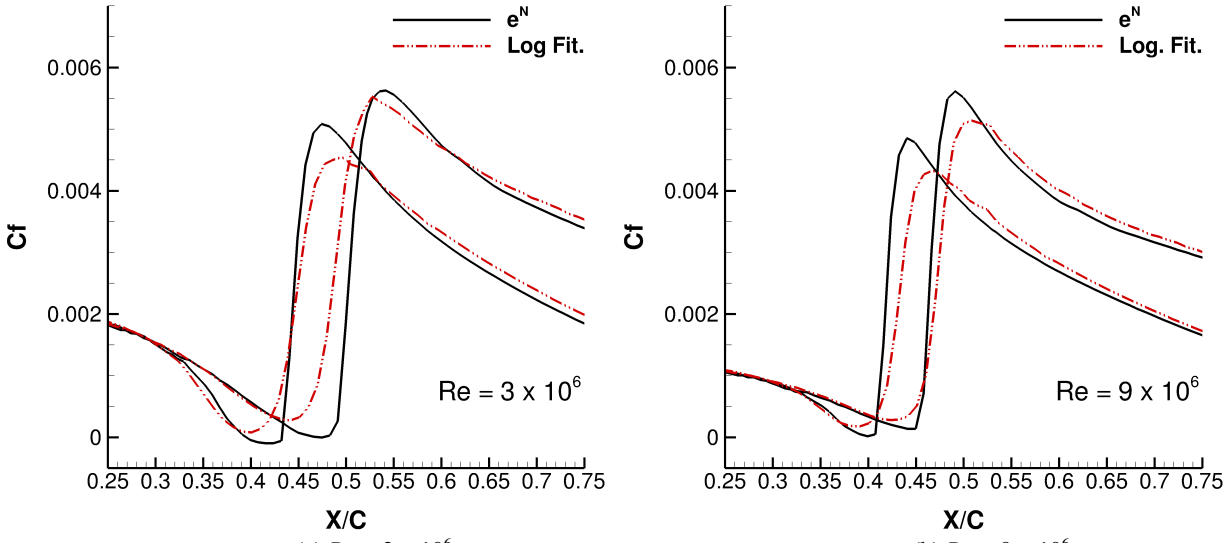

(a) $Re = 3 \times 10^6$.

(b) $Re = 9 \times 10^6$.

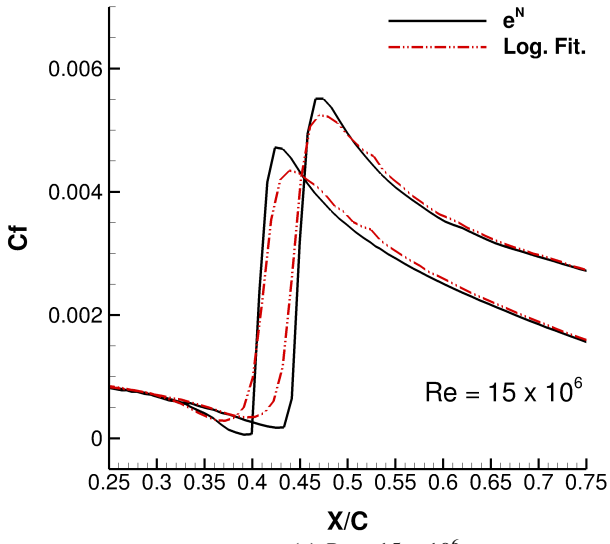

(c) $Re = 15 \times 10^6$.

Figure 8 – Skin friction coefficient, C_f, at various Reynolds numbers: effect of the proposed logarithm curve fitting on the predicted transition region. DU00-w-212 aerofoil at $Ma = 0.1$ and free-stream $Tu = 0.0816\%$ and $\mu_t/\mu = 10.0$.

Increasing the free-stream turbulent kinetic energy by one order, i.e. $Tu = 0.2582\%$, the predictions obtained employing the logarithm curve fitting in the one-equation LCTM are still in good agreement with Xfoil results, as seen in figures 8a-c, and no further calibration of the transition onset was required. At even higher free-stream turbulence intensity, $Tu = 0.8165\%$, results shown in figures 8a-c indicate that the proposed modified model agrees with Xfoil at Reynolds numbers $Re = 3 \times 10^6$ and $Re = 9 \times 10^6$, while at $Re = 15 \times 10^6$ it predicts an earlier transition point. This shows that further investigations may be required for high levels of free-stream turbulence intensity at very high Reynolds numbers. In fact, the original model [15] has been already calibrated and assessed for a large range of free-stream turbulence intensities spanning from $Tu = 0.03\%$ to $Tu = 7\%$ but at intermediate Reynolds number, 50×10^3 and 500×10^3. However, at high levels of free-stream turbulence intensity and very high Reynolds the flow is expected to be fully-turbulent due to surface roughness, erosion and dirt. Thus, employing a transition model at these extreme conditions may be questionable.

When employed to predict lift and drag coefficients at various angles of attack, the $\gamma-$equation LCTM with the logarithm curve fitting for the transition onset, shows good agreement with Xfoil computations as seen from figures 11a-b for $Re = 3 \times 10^6$, figures 12a-b for $Re = 9 \times 10^6$ and figures 13a-b for $Re = 15 \times 10^6$. As expected the original model predicts an earlier transition and thus a much higher drag coefficient, in particular at low angles of attack, for the two higher Reynolds numbers considered, while the proposed calibrated model shows better agreement with Xfoil capturing the low drag bucket. At the highest Reynolds number considered, 15×10^6, the original model does not even predict a low drag bucket while employing the logarithm curve fitting for the transition onset, more reliable results are obtained as can be seen in figure 13b. Tables 3, 4 and 5 summarise some important design properties computed for the DU00-w-212 aerofoil such as the low drag bucket extension, the zero lift angle ($\alpha_{Cl=0}$) and the lift slope (Cl_α). Note that Cl_α is computed here using the lift coefficients at -4° and 4° angles of attack. In comparison with Xfoil results; the low drag bucket extension as well as the zero lift angle are correctly predicted, less than 1% difference, by the calibrated model for all cases considered, while the original transitional model leads to reliable results only for $Re = 3 \times 10^6$. Regarding the Cl_α, slightly lower, around 3%, values are predicted by both models.

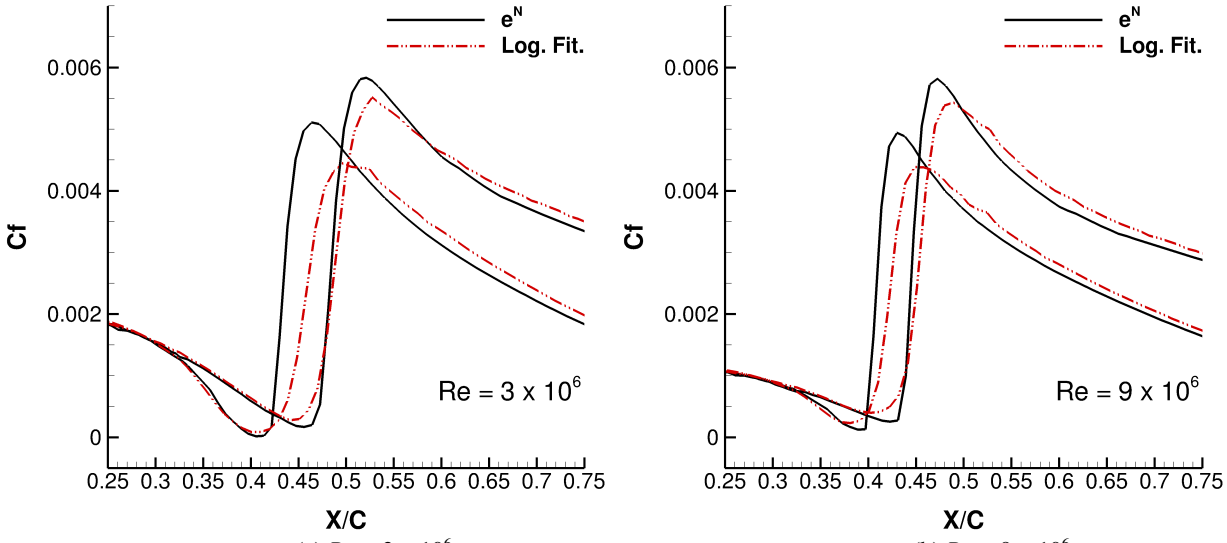

(a) $Re = 3 \times 10^6$.

(b) $Re = 9 \times 10^6$.

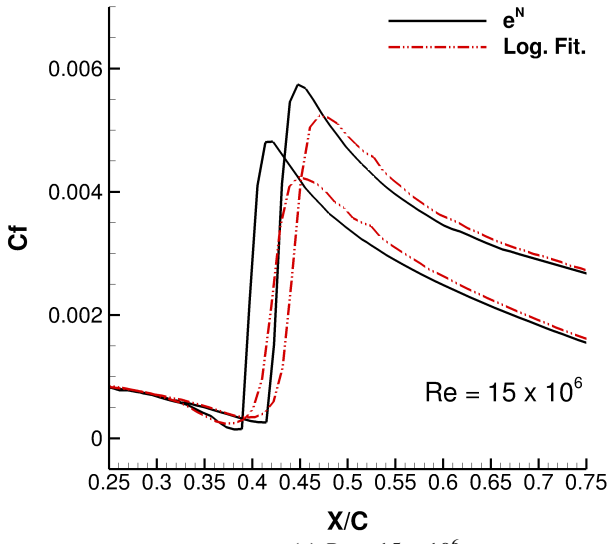

(c) $Re = 15 \times 10^6$.

Figure 9 – Skin friction coefficient, C_f, at various Reynolds numbers: effect of the proposed logarithm fitting on the predicted transition region. DU00-w-212 aerofoil at $Ma = 0.1$ and free-stream $Tu = 0.2582\%$ and $\mu_t/\mu = 10.0$.

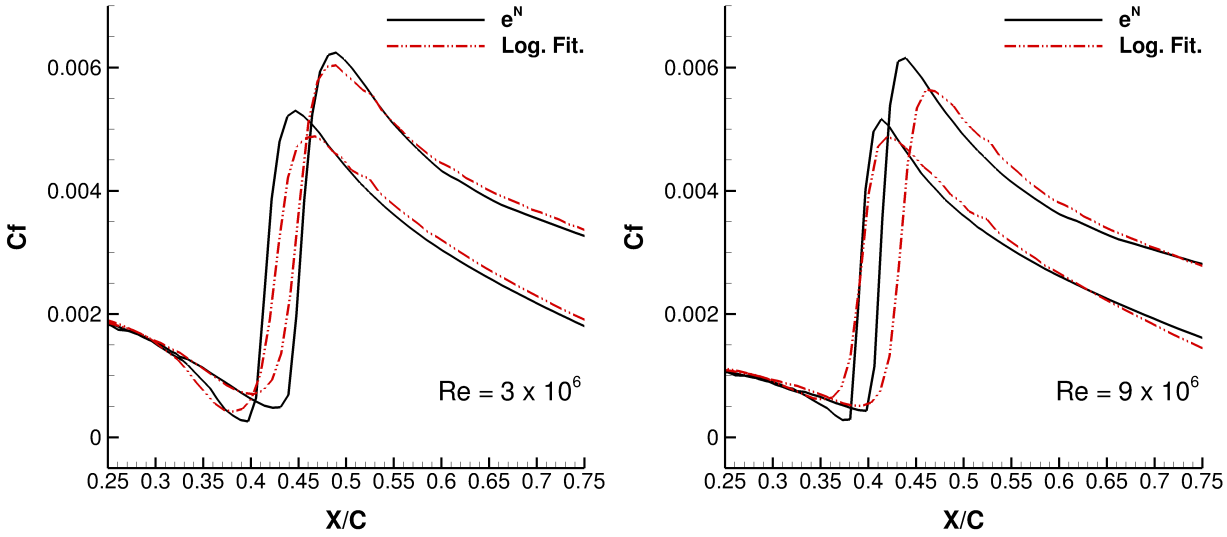

(a) $Re = 3 \times 10^6$.

(b) $Re = 9 \times 10^6$.

(c) $Re = 15 \times 10^6$.

Figure 10 – Skin friction coefficient, C_f, at various Reynolds numbers: effect of the proposed logarithm fitting on the predicted transition region. DU00-w-212 aerofoil at $Ma = 0.1$ and free-stream $Tu = 0.8165\%$ and $\mu_t/\mu = 10.0$.

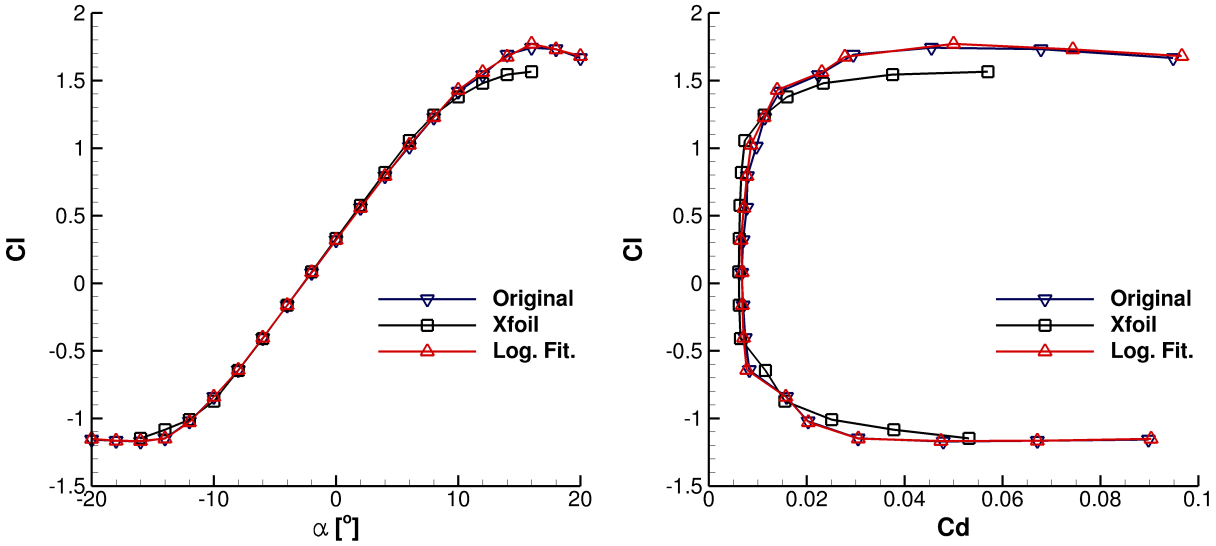

(a) Cl vs α. (b) Cl vs Cd.

Figure 11 – Polars for DU00-w-212 aerofoil at $Re = 3 \times 10^6$, $Ma = 0.075$ and free-stream $Tu = 0.0864\%$ and $\mu_t/\mu = 1.0$.

	Xfoil	Log. Fit.	Original
low drag bucket extension	$6° \div -6°$	$6° \div -8°$	$4° \div -8°$
$\alpha_{Cl=0}$	$-2.69°$	$-2.66°$	$-2.65°$
Cl_α	0.123	0.120	0.120

Table 3 – Summary of the DU00-w-212 aerofoil design properties at $Re = 3 \times 10^6$, $Ma = 0.075$ and free-stream $Tu = 0.0864\%$ and $\mu_t/\mu = 1.0$.

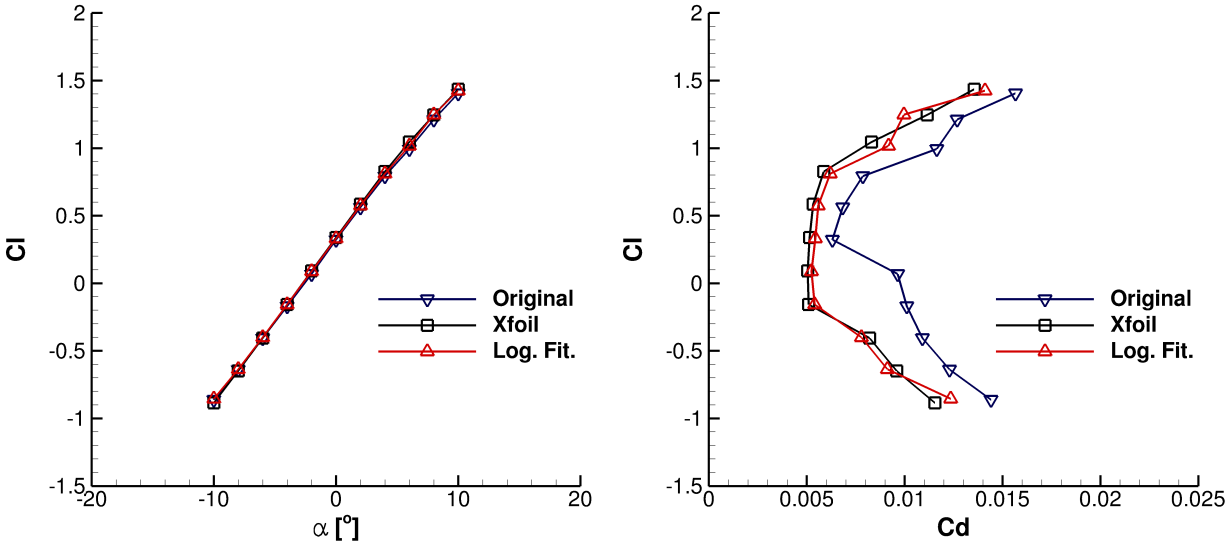

(a) Cl vs α. (b) Cl vs Cd.

Figure 12 – Polars for DU00-w-212 aerofoil at $Re = 9 \times 10^6$, $Ma = 0.082$ and free-stream $Tu = 0.1988\%$ and $\mu_t/\mu = 10.0$.

	Xfoil	Log. Fit.	Original
low drag bucket extension	$4° \div -4°$	$4° \div -4°$	$4° \div 0°$
$\alpha_{Cl=0}$	$-2.74°$	$-2.73°$	$-2.58°$
Cl_α	0.123	0.121	0.120

Table 4 – Summary of the DU00-w-212 aerofoil design properties at $Re = 9 \times 10^6$, $Ma = 0.082$ and free-stream $Tu = 0.1988\%$ and $\mu_t/\mu = 10.0$.

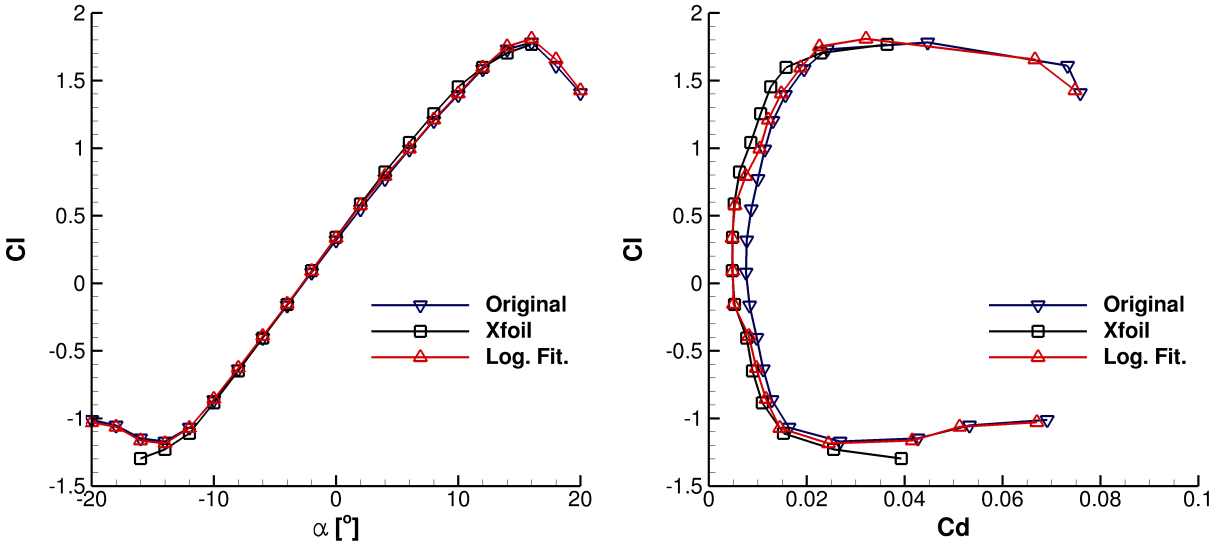

(a) Cl vs α. (b) Cl vs Cd.

Figure 13 – Polars for DU00-w-212 aerofoil at $Re = 15 \times 10^6$, $Ma = 0.08$ and free-stream $Tu = 0.3346\%$ and $\mu_t/\mu = 10.0$.

	Xfoil	Log. Fit.	Original
low drag bucket extension	$4° \div -2°$	$4° \div -2°$	Failed to predict
$\alpha_{Cl=0}$	$-2.75°$	$-2.74°$	$-2.65°$
Cl_α	0.123	0.119	0.117

Table 5 – Summary of the DU00-w-212 aerofoil design properties at $Re = 15 \times 10^6$, $Ma = 0.08$ and free-stream $Tu = 0.3346\%$ and $\mu_t/\mu = 10.0$.

In the original paper of Somers [37] which describes the design of the NLF(1)-0416 aerofoil, both theoretical and experimental results are provided. Here the wind tunnel data are used to evaluate the model predictions for this aerofoil at $Re = 4 \times 10^6$. As can be seen from figures 14a-c the original and calibrated models give reliable results for lift and drag coefficients, as well as, for the transition position on both sides of the aerofoil. It has to be noted that at the Reynolds number considered for this test case, equation (7) give a value $C_{Onset1} = 2.63$ thet is not much different than the one employed in the original model. However, the proposed calibration leads to a slightly better agreement with the experimental data.

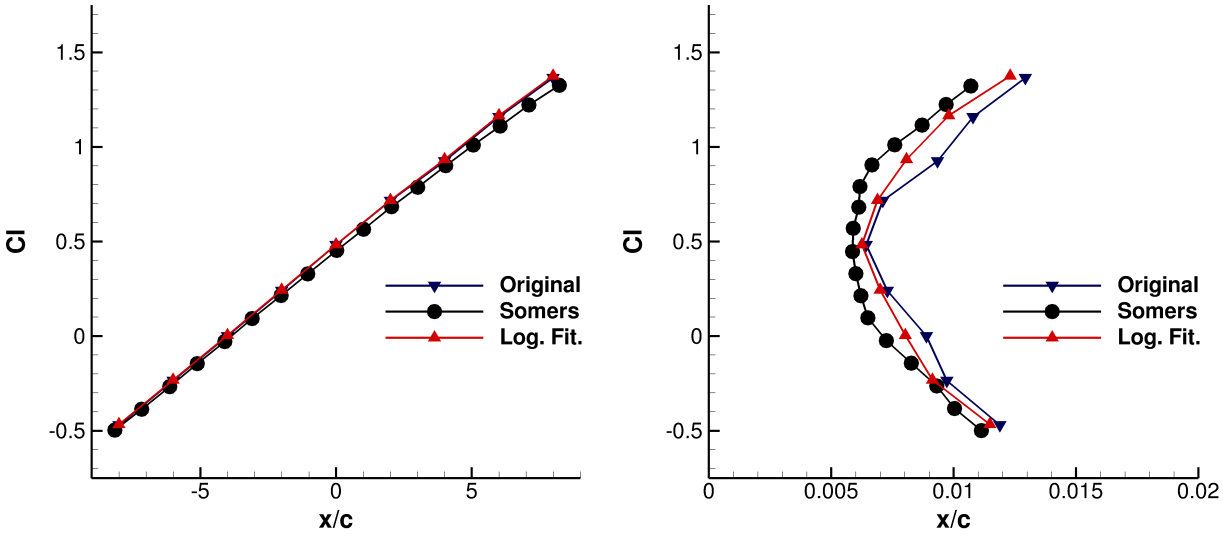

(a) Cl vs α.

(b) Cl vs Cd.

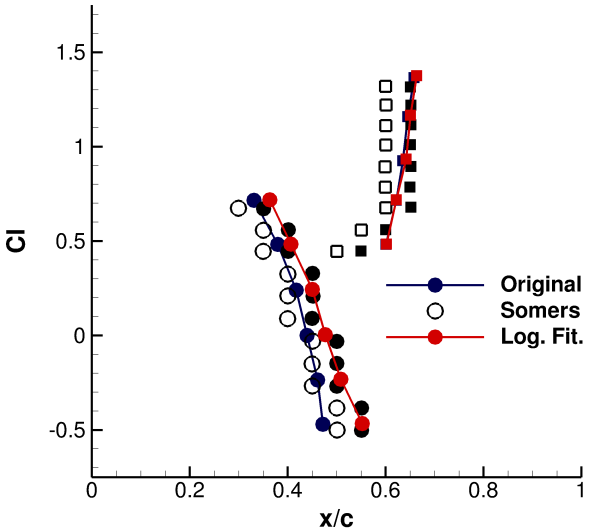

(c) X_{tr}/c vs Cl.

Figure 14 – Polars and transition position, X_{tr}, for the NLF(1)-0416 aerofoil at $Re = 4 \times 10^6$, $Ma = 0.1$ and free-stream $Tu = 0.0816\%$ and $\mu_t/\mu = 10.0$. Experimental results form Somers [37] . ◯ - upper surface and □ - lower surface.

3-D Cases

Finally, the tuned model has been employed to predict the flow around the AVATAR wind turbine blade presented in section 4 at three different wind speeds. In all cases, a free-stream $Tu = 0.0816\%$ and $\mu_t/\mu = 10.0$ have been used. For three-dimensional simulations there is no unique way to define the Reynolds number to be employed to evaluate the transition onset. However, since it is well known that for rotary wings the main contribution to the aerodynamic forces is generated in the region around the section at 75% radius; the local Reynolds number at this station, computed as

$$Re_{75\%R} = \frac{\rho_\infty \sqrt{{U_W}^2 + (0.75R \cdot \mathrm{RPM} \cdot \pi/30)^2} \cdot c_{\,75\%R}}{\mu} \tag{8}$$

has been employed in equation (6) to compute the C_{Onset1} employed in the simulations. Table 6 show the predicted Power and Thrust produced by the wind turbine blade for the considered conditions. As expected, when laminar to turbulent transition is considered an increase of power and thrust of about $15-20\%$ and $8-10\%$, respectively, is obtained with respect to fully-turbulent results. Moreover, when fully-turbulent flow is considered a decrease in the performance of the blade is observed at wind speed higher than the design point of $U_W = 10.5m/s$. Contours of C_f on the suction and pressure side of the blade are presented in figures 15a-c and 16a-c. The transition position is around half of the chord in the region around 75% radius on both pressure and suction sides. However, towards the blade root the transition position moves towards the LE on the suction side and the TE on the pressure side as result of the effect of the lower rotational speed on the local angle of attack.

	Fully-Turbulent Flow			Transitional Flow		
U_W (m/s)	10.0	10.5	12.0	10.0	10.5	12.0
Power (KW)	8150.97	9469.98	9038.53	9432.87	10925.75	10837.78
Thrust (KN)	1228.55	1357.60	1048.42	1331.98	1473.83	1155.48

Table 6 – Power and Thrust as function of the wind speed, U_W, for the AVATAR wind turbine blade with fully-turbulent and transitional flow assumptions.

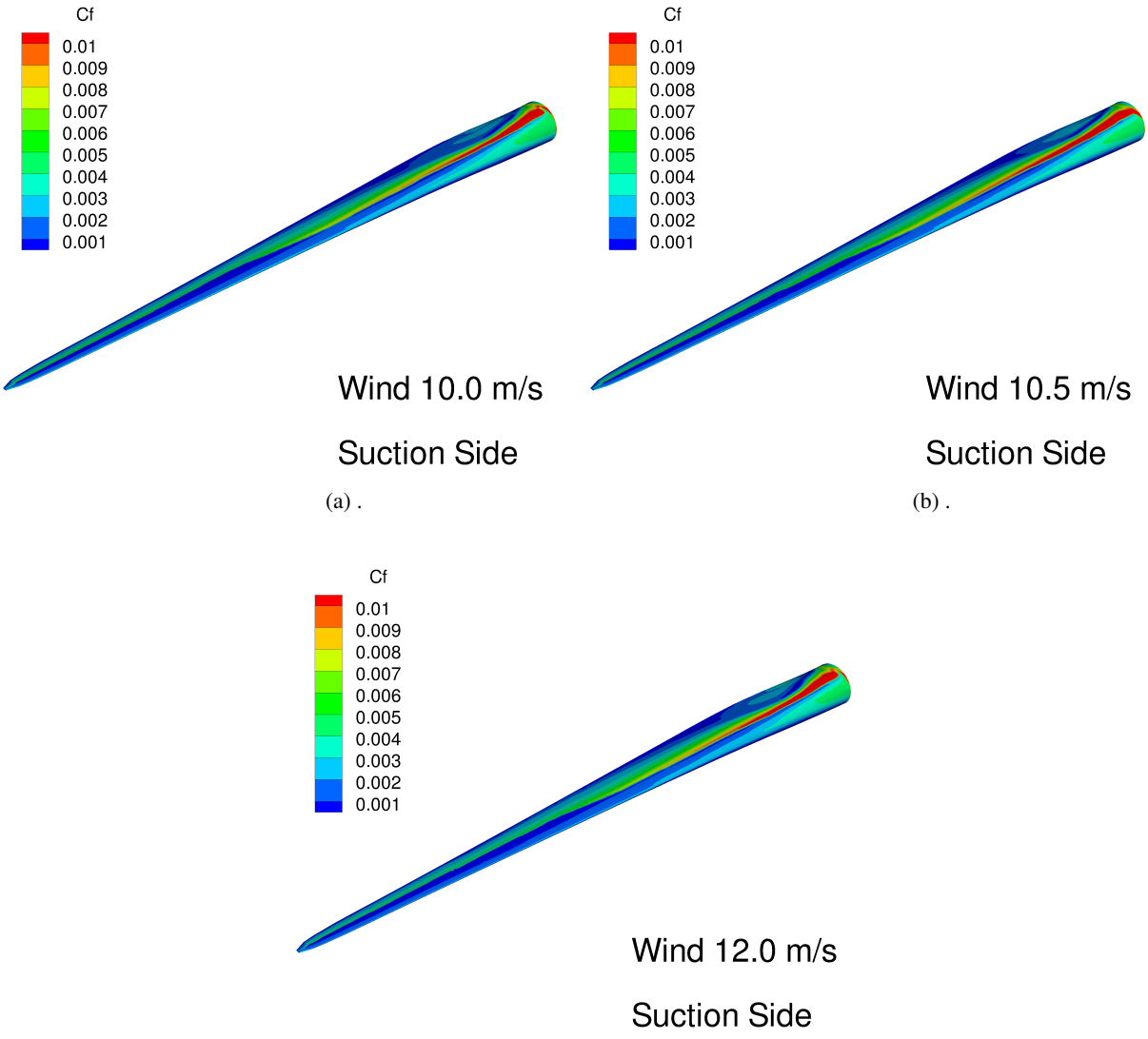

(a) .

(b) .

(c) .

Figure 15 – Skin friction coefficient contours for the suction side of the AVATAR wind turbine blade at different wind conditions.

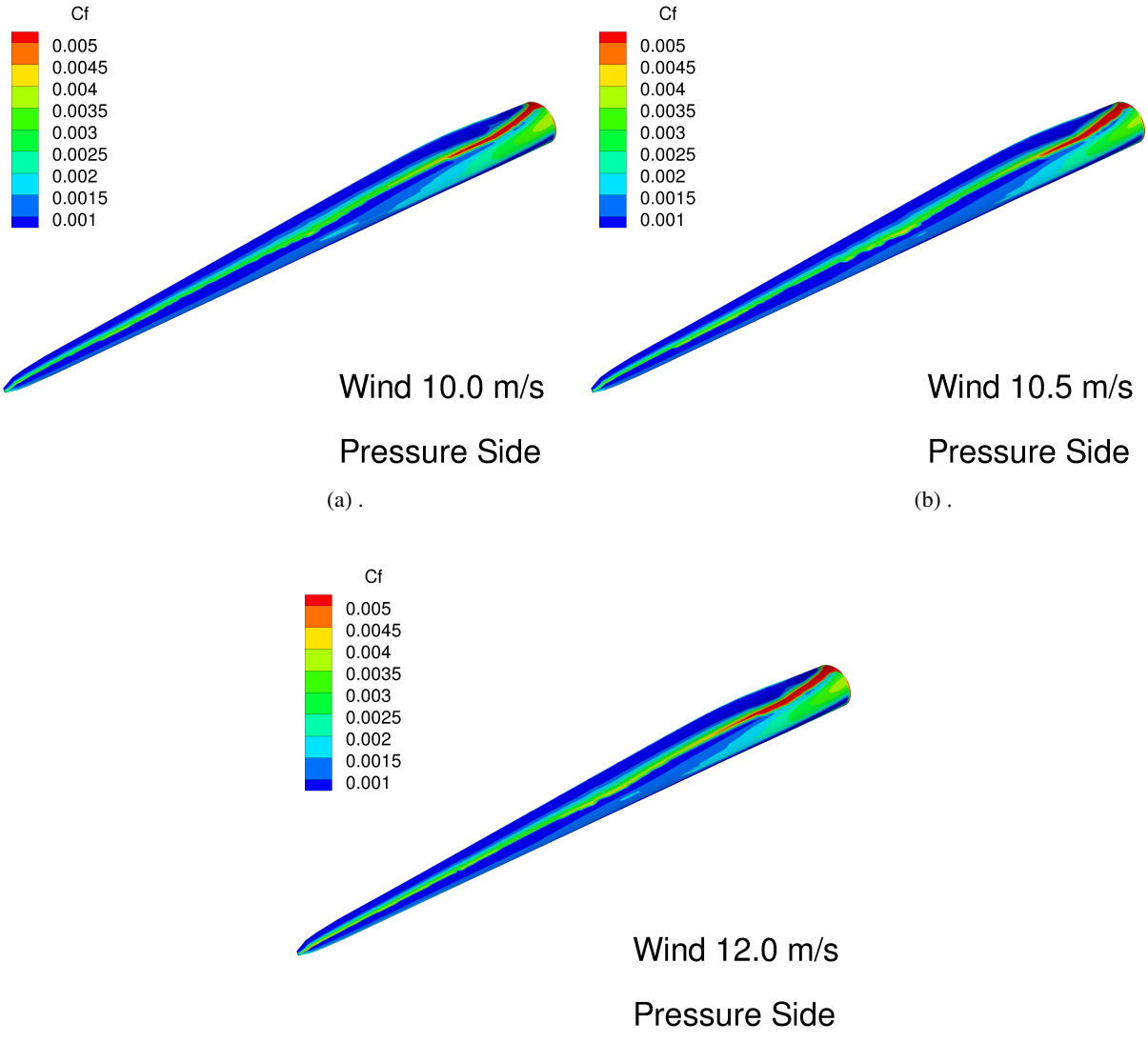

Figure 16 – Skin friction coefficient contours for the pressure side of the AVATAR wind turbine blade at different wind conditions.

Conclusions and Future Works

The LCTM concept was introduced by Menter et. al. [13] almost a decade ago to include transitional flows modeling in general-purpose CFD codes. This due to the fact that the commonly employed e^N method requires a complex infrastructure that limit its applicability in complex CFD simulations. Recently, a simplified version of model has been presented [15] reducing the formulation to only the γ-equation providing tunable coefficients to match the required application. The model has been assessed for various test cases however, further works are needed to evaluate the γ-equation model at more extreme conditions such as high Reynolds numbers (i.e. $Re \geq 1 \times 10^6$), very low Reynolds numbers (i.e. $Re \leq 50 \times 10^3$) and supersonic/hypersonic flows.

In this paper the, $\gamma-$equation transition model is calibrated for all Reynolds numbers flows, at low Mach numbers, to be employed in wind turbine applications. The calibration process consisted in a rescaling of C_{TU1} and C_{TU2} in equation (4) from 100.0 and 1000.0 to 163.0 and 1002.25, respectively, and a logarithmic curve has been proposed to define the transition onset, C_{Onset1}, as a function of the Reynolds number for $1 \times 10^6 \leq Re \geq 15 \times 10^6$. The proposed improvements to the model shown promising results for both two-dimensional and three-dimensional flows, even if cross-flow instabilities are neglected and only natural transition, i.e. $Tu < 1\%$, has been considered. Compared to the original model at high Reynolds numbers, while the latter displays a decay of the accuracy, the proposed calibrated model maintains a good level of reliability and retains the accuracy of the original model at lower Re. This shows that the original model can be improved and in future works further transitional effects such as cross-flow instabilities and high-Mach effect could be included.

Acknowledgments

Results were obtained using the EPSRC founded ARCHIE-WeSt High Performance Computer (www.archie-west.ac.uk). EPSRC grant no. EP/K000586/1. Simone Colonia is supported by the AVATAR project (FP7-ENERGY-2013-1/N608396). Vladimir Leble is supported by the MARE-WINT project (FP7-PEOPLE-2012-ITN/309395).

Nomenclature

C	Chord
Cd	Drag coefficient
C_f	Skin friction coefficient
Cl	Lift coefficient
Cl_α	Lift coefficient slope
Cl_{max}	Maximum lift coefficient
H	Boundary layer shape factor
k	Turbulent kinetic energy
Ma	Mach number
$\mathbf{P}$	Primitive variables vector
$\mathbf{R}$	Residual vector
R	Radius
Re_θ	Momentum-thickness Reynolds number, $\rho U_0 \theta/\mu$
Re_{θ_c}	Critical Momentum-thickness Reynolds number
Re_v	Strain-rate (or vorticity) Reynolds number $\rho S y^2/\mu$
S	Strain-rate absolute valure $(2S_{ij}S_{ij})^{1/2}$
S_{ij}	Strain-rate tensor $0.5(\frac{\partial u_i}{\partial x_j} + \frac{\partial u_j}{\partial x_i})$
Tu	Turbulence intensity, $100\sqrt{(2k/3)}/U$
Tu_L	Local turbulence intensity
u_i	Velocity component in the i-direction
U_W	Wind speed
U_0	Local freestream velocity
$\mathbf{W}$	Conservative variables vector
x_i	Spatial coordinate in the i-direction
X_{tr}	Transition position
y	Nearest wall distance
$\alpha_{Cl=0}$	Zero lift angle
γ	Intermittency
$\lambda_{\theta L}$	Local pressure gradient parameter
μ_t	Eddy viscosity
μ	Molecular viscosity
ω	Turbulence dissipation rate

Acronyms

AUSM	Advection Upstream Splitting Method
CF	Cross-Flow
CFD	Computatinal Fluid Dynamics
DNS	Direct Numerical Simulation
GCG	Generalised Conjugate Gradient
ILU	Incomplete Lower Upper factorisation
LCTM	Local-Correlation based Transition Modelling
LE	Leading edge
LES	Large Eddy Simulation
LM-Roe	Low Mach Roe
MUSCL	Monotone Upstream-Centred Scheme for Conservation Laws
NS	Nevier-Stokes
RANS	Reynold Averaged Nevier-Stokes
RPM	Rotations per minute
TE	Trailing edge
TS	Tollmien-Schlichting

References

[1] Aupoix, B., Arnal, D., Bezard, H., Chaouat, B., Chedevergne, F., Deck, S., Gleize, V., Grenard, P., and Laroche, E., "Transition and Turbulence Modeling," *Aerospace Lab Journal*, Vol. 2, 2011.

[2] Smagorinsky, J., "General Circulation Experiments with the Primitive Equations," *Monthly Weather Review*, Vol. 91, No. 3, 1963, pp. 99–164.

[3] Smith, A. and Gamberoni, N., "Transition, Pressure Gradient and Stability Theory," *Report No. ES 26388 - Douglas Aircraft Co.*, 1956.

[4] van Ingen, J., "A Suggested Semi-Empirical Method for the Calculation of Boundary Layer Transition Region," *Report No UTH-74 - Delft University of Technology*, 1956.

[5] Abu-Ghannam, B. and Shaw, R., "Natural Transition of Boundary Layers - The Effects of Turbulence, Pressure Gradient and Flow History," *Journal of Mechanical Engineering Science*, Vol. 22, No. 5, 1980, pp. 213–228.

[6] Michel, R., "Etude de la Transition sur les Profils d'Aile, Etablissement d'um Critere de Determination du Point de Transition et Calcul de la Trainee de Profil Incompressible," *Technical Report 1/1578A - ONERA*, 1951.

[7] Cebeci, T. and Smith, A., *Analysis of Turbulent Boundary Layers*, Academic Press, New York, 1974.

[8] Dhawan, S. and Narasimha, R., "Some Properties of Boundary Layer During the Transition from Laminar to Turbulent Flow Motion," *Journal of Fluid Mechanics*, Vol. 3, 1958, pp. 418–436.

[9] Gostelow, J., Blunden, A., and Walker, G., "Effects of Free-Stream Turbulence and Adverse Pressure Gradients on Boundary Layer Transition," *Journal of Turbomachinery*, Vol. 116, 1994, pp. 392–404.

[10] Steelant, J. and Dick, E., "Modelling of Bypass Transition with Conditioned Navier-Stokes Equations Coupled to an Intermittency Transport Equation," *International Journal for Numerical Methods in Fluids*, Vol. 23, 1996, pp. 193–220.

[11] Suzen, Y. and Huang, P., "Modeling of Flow Transition Using an Intermittency Transport Equation," *Journal of Fluids Engineering*, Vol. 122, 2000, pp. 273–284.

[12] Cho, J. and Chung, M., "A $k-\epsilon-\gamma$ Equation Turbulence Model," *Journal of Fluid Mechanics*, Vol. 237, 1992, pp. 301–322.

[13] Menter, F., Langtry, R., and Völker, S., "Transition Modelling for General Purpose CFD Codes," *Flow Turbulence and Combustion*, Vol. 77, 2006, pp. 277–303.

[14] Langtry, R. and Menter, F., "Correlation-Based Transition Modelling for Unstructured Parallelised Computational Fluid Dynamics Codes," *AIAA Journal*, Vol. 47, No. 12, 2009, pp. 2894–2906.

[15] Menter, F., Smirnov, P.E. Tao, L., and Avancha, R., "A One-Equation Local Correlation-Based Transition Model," *Flow Turbulence and Combustion*, Vol. 95, No. 4, 2015, pp. 583–619.

[16] Snel, H., "Review of the present status of rotor aerodynamics," *Wind Energy*, Vol. 1, 1998, pp. 46–69.

[17] Brodeur, R. and van Dam, C., "Transition Prediction for a Two-Dimensional Reynolds-averaged Navier–StokesMethod Applied to Wind Turbine Airfoils," *Wind Energy*, Vol. 4, 2001, pp. 61–75.

[18] Sørensen, N., "CFD Modelling of Laminar-turbulent Transition for Airfoils and Rotors Using the γ-Re_θ Model," *Wind Energy*, Vol. 12, No. 8, 2009, pp. 715–733.

[19] Khayatzadeh, P. and Nadarajah, S., "Laminar-Turbulent Flow Simulation for Wind Turbine Profiles Using the γ-Re_θ Transition Model," *Wind Energy*, Vol. 17, 2014, pp. 901–918.

[20] Lawson, S.-J., Steijl, R., Woodgate, M., and Barakos, G., "High Performance Computing for Challenging Problems in Computational Fluid Dynamics," *Progress in Aerospace Science*, Vol. 52, 2012, pp. 19–29.

[21] Barakos, G., Steijl, R., Badcock, K., and Brocklehurst, A., "Development of CFD Capability for Full Helicopter Engineering Analysis," *31st European Rotorcraft Forum*, 2005, pp. Paper No. 91, 19–29.

[22] Axelsson, O., "Conjugate Gradient Type Methods for Unsymmetric and inconsistent System of Linear Equation." *Linear Algebra and its Applications*, Vol. 29, 1980, pp. 1–16.

[23] Meijerink, J. and van der Vorst, H., "Guidelines for the Usage of Incomplete Decompositions in Solving Sets of Linear Equations as They Occur in Practical Problems." *Journal of Computational Physics*, Vol. 44, No. 1, 1981, pp. 134–155.

[24] Roe, P., "Approximate Riemann Solvers, Parameter Vectors and Difference Schemes," *Journal of Computational Physics*, Vol. 43, 1981, pp. 357–372.

[25] Osher, S. and Chakravarthy, S., "Upwind Schemes and Boundary Conditions with Applications to Euler Equations in General Geometries," *Journal of Computational Physics*, Vol. 50, No. 3, 1983, pp. 447–481.

[26] Rieper, F., "A Low-Mach Number Fix for Roe's Approximate Riemann Solver," *Journal of Computational Physics*, Vol. 230, 2011, pp. 5263–5287.

[27] Liou, M.-S., "The Evolution of AUSM Schemes," *Defense Science Journal*, Vol. 60, No. 6, 2010, pp. 606–613.

[28] Carrión, M., Woodgate, M., Steijl, R., and Barakos, G., "Implementation of all-Mach Roe-type Schemes in Fully Implicit CFD Solvers - Demonstration for Wind Turbine Flows," *International Journal for Numerical Methods in Fluids*, Vol. 73, No. 8, 2013, pp. 693–728.

[29] Colonia, S., Steijl, R., and Barakos, G., "Implicit Implementation of the AUSM$^+$ and AUSM$^+$up Schemes," *International Journal for Numerical Methods in Fluids*, Vol. 75, No. 10, 2014, pp. 687–712.

[30] van Leer, B., "Towards the Ultimate Conservative Difference Scheme, V. A Second Order Sequel to Godunov's Method," *Journal of Computational Physics*, Vol. 32, 1979, pp. 101–136.

[31] Van Albada, G., Van Leer, B., and Roberts, W., "A Comparative study of Computational methods in Cosmic Gas Dynamics," *Astronomy and Astrophysics*, Vol. 108, 1982.

[32] Menter, F., "Two-Equation Eddy-Viscosity Turbulence Models for Engineering Applications," *AIAA Journal*, Vol. 32, No. 8, 1994, pp. 1598–1605.

[33] Kato, M. and Launder, B., "The Modeling of Turbulent Flow Around Stationary and Vibrating Square Cylinders," *9th Symposium on Turbulent Shear Flows*, Kyoto, Japan 1993.

[34] Spalart, P. and Rumsey, C., "Effective Inflow Conditions for Turbulence Models in Aerodynamic Calculations," *AIAA Journal*, Vol. 45, No. 10, 2007, pp. 2544–2553.

[35] AVATAR project, "FP7-ENERGY-2013-1/N608396," *http://www.eera-avatar.eu/*, pp. accessed 05/2016.

[36] Drela, M. and Giles, M., "Viscous-Inviscid Analysis of Transonic and Low Reynolds Number Airfoils," *AIAA Journal*, Vol. 25, 1987, pp. 1347–1355.

[37] Somers, D., "Design and Experimental Results for a Natural-Laminar-Flow Airfoil for General Aviation Applications," *NASA Technical Paper*, Vol. 1861, 1981.